Stern Flow Hydrodynamics around a Self-propelled Maneuvering VLCC Ship

Oana Marcu
Progressive Ship Design, Romania
progressiveshipdesign@gmail.com

Elena-Gratiela Robe-Voinea
Mircea cel Batran Naval Academy, Romania
elena.robe@anmb.ro (corresponding author)

Received: 24 April 2024 | Revised: 23 May 2024 | Accepted: 25 May 2024

 DOI: https://doi.org/10.48084/etasr.7624

ABSTRACT

The present research explores the stern flow hydrodynamics around a maneuvering ship. Utilizing Computational Fluid Dynamics (CFD) techniques, several flow scenarios including different drift angles and propulsion configurations are modeled for the benchmark ship KRISO Very Large Crude Carrier 2 (KVLCC2). The analysis depicts all vortical structures that appear in the propeller operating area, explaining their formation and evolution. Also, the mutual interactions between the turbulent flow and the propulsion unit are observed and examined. The detailed outcome is intended to provide valuable insights for both new ship design and retrofits, aiming to advance new and sustainable engineering practices.

Keywords-KVLCC2; RANS; vortical flow; maneuvering

I. INTRODUCTION

On the background of the major concern raised by the continuously increasing level of greenhouse gas (GHG) emissions from ships, the International Maritime Organization (IMO) has set the ambitious target to achieve net zero emissions from ships by 2050.

Though the economic and geopolitical scene of nowadays is not the best, a minimum 2% growth in maritime trade volume was predicted for 2024-2028, with the increase being more obvious if referred on a ton-mile basis that will register an approximate 4% growth [3]. Although salutary from the economic point of view, these percentages directly influence the level of GHG emissions that represented 2.9% of the global emissions caused by human activities in 2018 and could increase by up to 130% of 2008 emissions by 2050 [4]. In light of these data, IMO developed a new greenhouse gas emissions reduction strategy [1]. Increasingly ambitious compared to the 2018 one, the new 2023 plan targets net zero emissions from ships by 2050.

These high expectations that come amid some of the greatest challenges of our time [5] and the present knowledge that, predominantly, relates the problem of GHG pollution from ships with the propulsion system, force the naval architect to prioritize its optimization [6]. This and the IMO requirement for a vessel to provide sufficient installed propulsion power to maintain maneuverability in adverse conditions [2], oblige a thorough understanding of the propeller operating field, on both straight ahead route or during maneuvering. Only a detailed image of the turbulent phenomena following the ship sailing at an angle of drift different from zero can lead to the best design choices for either new projects or retrofits, enabling the optimal solutions that can work towards GHG emissions reduction.

As explained in [7], when applying a rudder angle, the ship engages in a maneuvering motion that determines a "crossflow in the propeller plane" affecting the actual propeller performance and, following the ship speed-fuel consumption trajectory, the level of pollution. In conclusion, the paradigm of zero incidence must make room for the asymmetric flow and its influence on the overall efficiency of the propulsion system, with the thorough understanding of the turbulent stern flow during maneuvering being essential for achieving the IMO's ambitious net zero emissions target by 2050 amidst growing the maritime trade and lowering the GHG emissions.

A. Objective

According to the previous information, the present scientific research intends to provide a detailed evaluation of the development of stern flow around a maneuvering ship with or without propeller. Specifically, the analysis will focus on determining the vortex formations that appear in the propeller operating area and on examining the mutual interaction between the turbulent flow and the propulsion unit. The study wants to emphasize the need of this advanced type of knowledge in selecting or optimizing ship propulsion, for achieving the desired hydrodynamic performance while reducing GHG emissions and, in the end, pollution and climate change impact [5].

B. Benchmark Ship

Given the accent on the incident flow, particularly relevant for robust ships with significant block coefficients, the present study approaches the 1:58 scale model of the KRISO Very Large Crude Carrier 2 (KVLCC2) [8-12] (Figure 1).

Fig. 1. The KRISO Very Large Crude Carrier 2.

Belonging to the class of single screw tankers with bulbous bow and stern bulb, the KVLCC2 hull was design by Maritime and Ocean Engineering Research Institute (MOERI). The full-bodied ship defined by a large block coefficient, low speed and complicated geometry that generates high velocity and pressure gradients was proposed as benchmark ship at various workshops on ship hydrodynamics and ship maneuverability [8-12]. Additionally, the research considered the KP458 right-hand fixed pitch propeller designed by MOERI.

II. NUMERICAL MODELLING

For achieving the objective of this paper, a detailed research that employed Computational Fluid Dynamics (CFD) techniques was conducted. Used for a multitude of engineering applications that study all kinds of fluids and their motion [13, 14], the CFD type approach is becoming highly popular in the ship hydrodynamics field. Drawn for the first time within the Gothenburg 2000 workshop [8], the research direction that approaches the study of the incident flow developed around a hull with or without propeller was pursued by a cadre of renowned researchers. Notably, authors in [15-17] systematically studied the incident flow developed around the self-propelled Esso Osaka tanker hull. Authors in [18] analyzed the static drift and dynamic maneuvers of the fully appended KVLCC2 tanker ship. Authors in [19] implemented the actuator disc theory for solving the propulsion performance of a maneuvering tanker hull, whereas authors in [20] numerically considered the flow around the KVLCC2 hull in static drift motion and authors in [7, 21, 22] evaluated the effects of drift angle on a self-propelled ship.

A. Modelling Conditions

It is worth noting that the following results represent just a fraction of a comprehensive study aimed at gaining deeper insights into stern flow hydrodynamics. The complete analysis involved 63 simulations that produced an equal number of numerical results. Due to the high complexity of the subject and taking into account the space constraints, only a subset of these solutions is showcased in this article.

Following the experimental data given by MOERI [8], the extensive study approached, in a numerical manner, a complete set of Planar Motion Mechanism (PMM) tests of "static drift," "static rudder" and "static drift and rudder" type. Detailed in [23], the Experimental Fluid Dynamics (EFD) procedure considers that the motion of the experimental model is forced through water at a given drift and/or rudder angle and the corresponding hydrodynamic forces and moments are measured. In complete accordance with [8], the entire numerical setup implied the next combinations:

- "static drift" tests for a range of drift angles (β), extended between -9° and 9° with 3° step;
- "static rudder" tests for a range of rudder angles (δR) varying with 10° step from -30° to 30°;
- "static rudder and drift" for all possible combinations drift angle - rudder angle.

Following the experimental procedure of MOERI [8] and considering the right-handed Cartesian system attached to the ship hull, the angle of drift is positive when turning the bow to the starboard side. As for the rudder angle, it does not follow the EFD modeling, with δR being positive when the rudder is banded towards portside.

Regarding the constructive configurations, each of the previously presented flow cases were defined for the:

- bare hull case,
- hull with propeller case, and
- hull with rudder and propeller case.

In order to reach the actual objective of this paper, only two of the seven defined "static drift" situations were approached, for both bare hull and hull with propeller case.

For a better understanding of the problem, Table I summarizes the flow cases - constructive configuration combinations examined in the subsequent analysis.

TABLE I. ANALYSIS CASES

Drift angle	$\beta = 0°$	$\beta = 9°$
Study configurations	bare hull	
	hull with propeller	

Conformable with the EFD analysis, the virtual PMM tests were conducted at a water temperature of 11.1° C, a scale model speed U of 1.047 m/s, and the right-hand propeller operating at a revolution of 8.59 rps. For the given parameters, the corresponding Froude and Reynolds numbers are equal to 0.142 and 4.6×10^6, respectively. Due to the small enough value of the Froude number, the computation neglected the free surface effect. In a supplementary way, the motion of the 1:58 KVLCC2 was restricted in both longitudinal and vertical direction.

B. Mathematical Model

The "static drift" type PMM tests were virtually modeled by using a Reynolds averaged Navier-Stokes (RANS) solver. The numerical integration of the incompressible RANS equations [23], coupled with the Explicit Algebraic Stress Model (EASM) turbulence model [24] facilitates the acquirement of the three-dimensional flow solution. The RANS – EASM coupling aims to solve the "closure problem" introduced by the averaging procedure of the continuity and momentum equations.

For modelling the propeller effect, a lifting line propeller model was implemented in the viscous CFD solver so that the forces and moments developed by the propulsion unit to be taken into account by a "body force" approach.

The partial differential equations governing the incident flow around the hull with or without propeller are resolved by applying the Finite Volume Method (FVM).

C. Boundary Conditions

As Figure 2 depicts, boundary conditions of Dirichlet and Neumann type are imposed for pressure, velocity, turbulent kinetic energy, and turbulent frequency on each face of the computational domain.

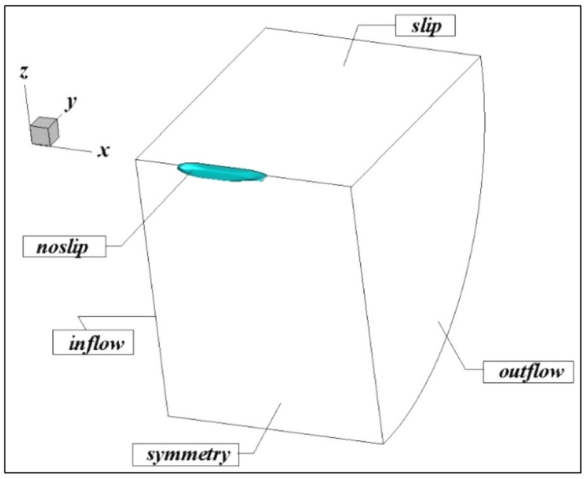

Fig. 2. Boundary conditions.

D. Computational Grids

A mono-block fully structured grid of H-O type returns the entire computational domain (Figure 3). The grid is concentrated toward the ship hull, in longitudinal and radial direction enabling minimum errors for velocity and pressure gradients.

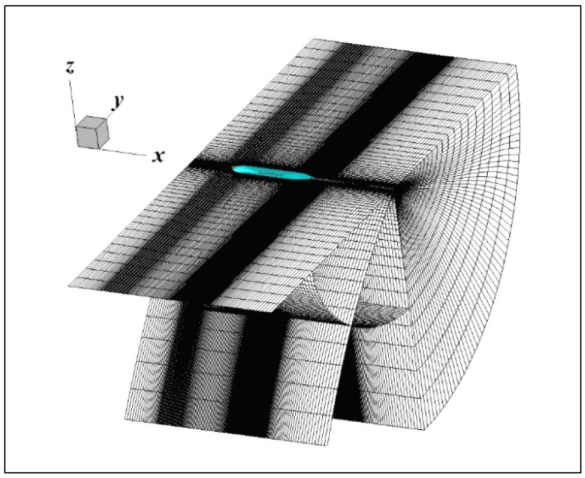

Fig. 3. Computational grid.

As revealed in Figure 4, for the propeller, the grid takes on a cylindrical shape. In this case, the structured three-dimensional domain functions as a substitute for the actual geometry of the propulsion unit considered by a "body force" approach.

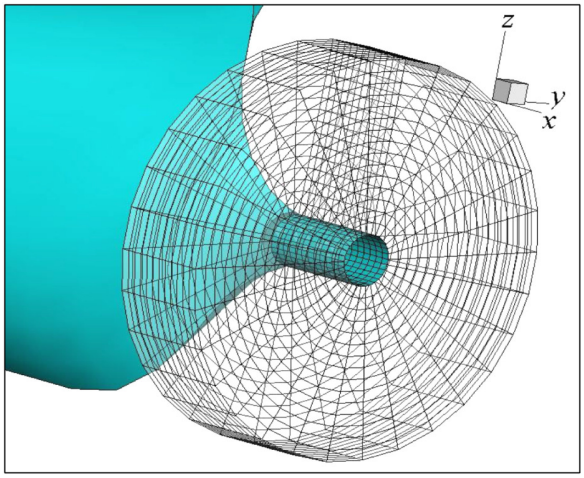

Fig. 4. Propeller computational grid.

The solutions of the aforementioned numerical procedure are intended to offer a computational response to the development of the turbulent flow in the propeller operating area, when the ship is on a straight route or engaged on a maneuver.

III. RESULTS AND DISCUSSIONS

Of major importance for the flow developed around a ship hull, the axial velocity distribution is, exclusively, addressed in this report. Following the research direction outlined in [9], the current paper will focus on examining five transversal sections longwise the ship in front of, at, and behind the propeller plane. Depicted in Figure 5, the sections are placed upstream of the propeller plane at 0.85 L_{pp} and 0.95 L_{pp} in the propeller plane, at 0.9825 L_{pp}, and downstream of the propeller plane at 1.00 L_{pp} and 1.10 L_{pp}.

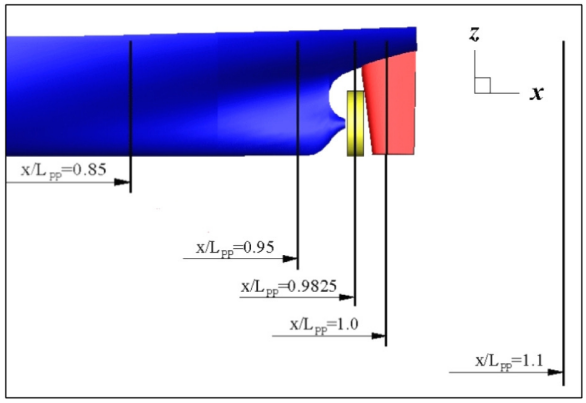

Fig. 5. Longitudinal position of the transverse sections considered for the axial velocity distribution.

As per [23] and based on the experimental results provided by [9, 25], the numerical methodology considered for the axial velocity distribution was qualitatively validated before starting the calculation. It thus highlighted the accuracy of the numerical technique supporting the continuation of the research. To provide the clearest understanding of the static maneuvering motion influence on the propulsion unit and vice versa, the results will be separately presented for the flow upstream, at the location, and downstream of the propeller disk plane.

A. Flow Upstream of the Propeller Plane

Figures 6 and 7 depict the axial velocity distribution upstream of the propeller plane at $x = 0.85\ L_{pp}$ and $x = 0.95\ L_{pp}$ for the situations detailed in Table I. The axial-symmetrical character of the flow with respect to the Center Line (CL, the xOz symmetry plane of the vessel) is underlined for the bare hull case when engaged on a straight ahead motion ($\beta = 0°$). Also, the presence of two counter-rotating vortical structures in the port and starboard boundary regions of the contour lines is revealed in Figures 6(a) and 7(a). In [23], the origin of the two formations in the bilge area was identified as downstream of $x = 0.70\ L_{pp}$.

When applying a non-zero drift angle, such as $\beta = 9°$, the starboard-portside observed symmetry of the flow disappears and the intensity of the boundary vortices changes. As shown in Figures 6(b) and 7(b), the level of these formations increases in diagonal direction of the incident flow and decreases in the incident board. In [23], it is explained that the origin of these high magnitude eddies moves from $x = 0.70\ L_{pp}$ toward the fore part of the vessel for increasing β. For $\beta = 9°$, the inception point of the abovementioned bilge vortices is identified at $x = 0.40\ L_{pp}$. Additionally, when $\beta \neq 0°$ a new turbulent manifestation found to originate in the bow area [23] appears in the board opposite to the incident board of the current amplifying the manifestation of the previous.

Analyzing the axial velocity at $x = 0.95\ L_{pp}$, a second pair of counter-rotating vortices is observed in the propeller disk area. The two formations will further generate the so-called "hook"-like shape that is usually observed in the flow pattern of very large tanker vessels on a straight route. Although hardly noticeable for zero incidence, the "hook" becomes pronounced in the starboard side when a portside drift angle is imposed to the hull. The forming of this new pair of eddies is attributed to the narrowing of the hull in the studied area along with the pronounced curvature of the stern bulb. Their origin is found to be the same as that of the bilge eddies [23]. Consequently, these turbulent presences reduce the values of the axial velocities in the disc area. As evidenced in Figure 7(a), the non-dimensional axial velocity, u, varies between 0.1 U at the propeller shaft and 0.5 U at the tip of the propeller blades.

For the hull with propeller case, Figure 6 reveals a velocity distribution that closely resembles the bare hull situation in terms of both placement and recorded values. The two previously identified groups of bilge vortices and their associated longitudinal manifestation are present in this case as well. Similar with the bare hull configuration, they have the same origin, in the bilge area, downstream of $x = 0.70\ L_{pp}$ for $\beta = 0°$ and $x = 0.40\ L_{pp}$ for $\beta = 9°$, but exhibit different evolutions [23]. The first group is directed to the bottom of the ship, converging towards the propeller plane and forming the "hook"-like shape, whereas the second group, identified in the boundary of the contour lines, evolves along the sides towards the free-surface. For non-zero incidence angles the third vortex that is formed in the bow area and developed in diagonal direction of the incident flow, is found. As in the bare hull analysis, its presence enhances the side-evolving eddy on its direction. It is obvious that the two structures are amplified on the side opposite to the incidence of the current, with both the intensity and longitudinal position of the origin being strongly dependent on the value of the drift angle.

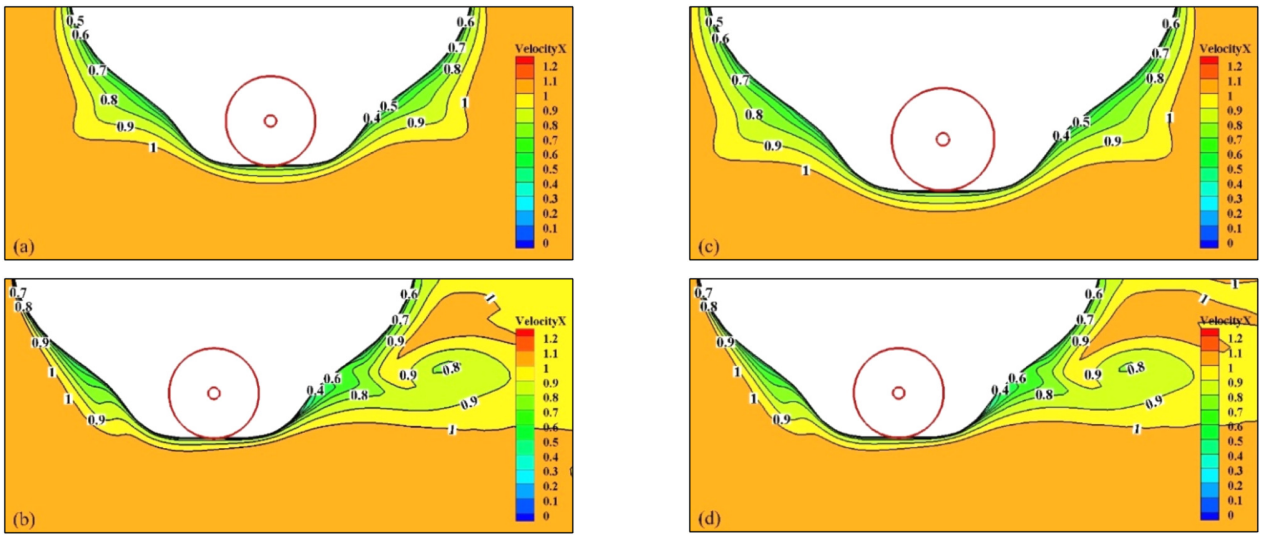

Fig. 6. Axial velocity distribution upstream of the propeller plane at $x = 0.85\ L_{pp}$ for: (a) bare hull and $\beta = 0°$, (b) bare hull and $\beta = 9°$, (c) hull with propeller and $\beta = 0°$, and (d) hull with propeller and $\beta = 9°$.

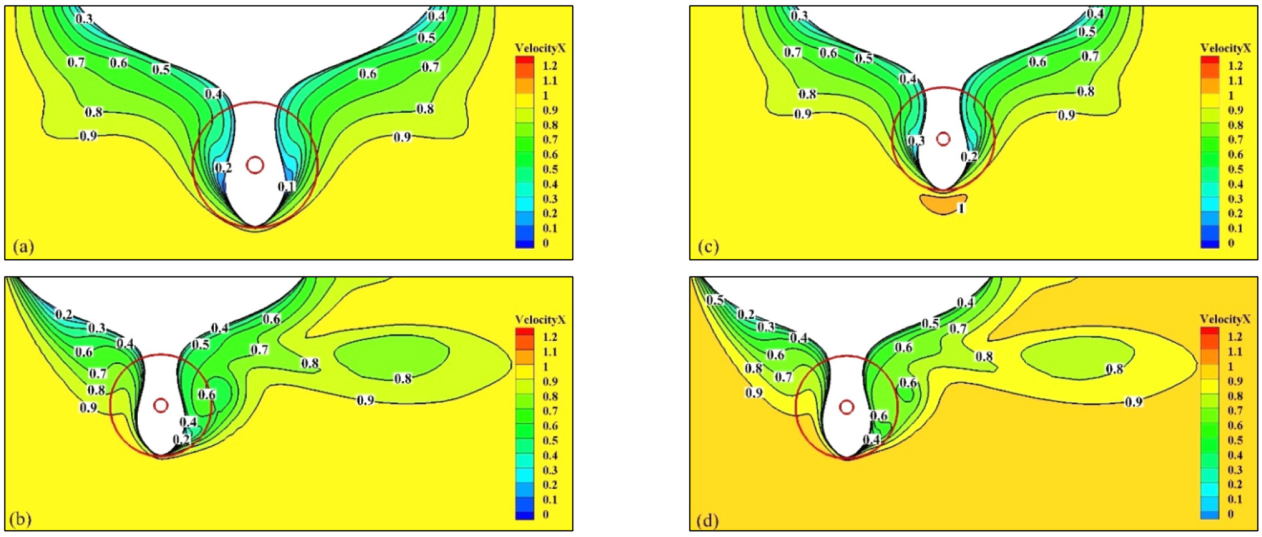

Fig. 7. Axial velocity distribution upstream of the propeller plane at $x = 0.95\ L_{pp}$ for:: (a) bare hull and $\beta = 0°$, (b) bare hull and $\beta = 9°$, (c) hull with propeller and $\beta = 0°$, and (d) hull with propeller and $\beta = 9°$.

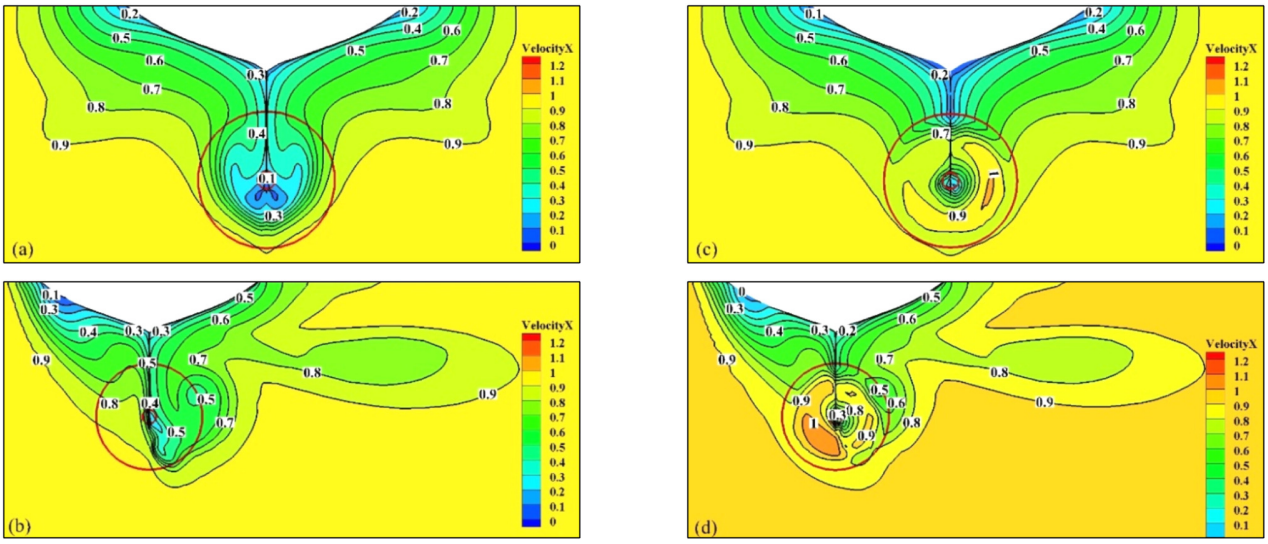

Fig. 8. Axial velocity distribution in propeller plane at $x = 0.9825L_{pp}$ for: (a) bare hull and $\beta = 0°$, (b) bare hull and $\beta = 9°$, (c) hull with propeller and $\beta = 0°$, and (d) hull with propeller and $\beta = 9°$.

Although the presence of the propeller is almost imperceptible outside the study area, at a close look, its rotational and propulsive effect can be observed. Thus, for $\beta = 0°$ and $x = 0.95\ L_{pp}$, at the bottom of the disc, the axial velocity of the fluid shows a slight increase, whereas for $\beta = 9°$ and $x = 0.95\ L_{pp}$ the unit diminishes the two bilge vortices on the side opposite to the incidence of the current. This acceleration of the flow in front of the propeller is associated with a pressure loss on the stern of the ship and, in the end, with the "suction" phenomenon known to be a growth factor for the ship resistance.

B. Flow in the Propeller Plane

Following the same pattern as for the study of the flow upstream of the propeller plane, Figure 8 depicts the axial velocity distribution in the actual section of the disc, at $x = 0.9825\ L_{pp}$ for the situations detailed in Table I. When studying the bare hull on a straight route ($\beta = 0°$), the flow keeps its symmetry with respect to the CL, with the two pairs of counter-rotating eddies being, once again, observed. If, regarding the structures manifested in the port and starboard boundary regions of the contour lines, there are no substantial changes compared to the upstream sections, the "hook"-like shape in the propeller disc area becomes more obvious. It is clear that the propeller is forced to operate in an intricate flow domain with reduced velocities due to the bilge vortices influences.

For $\beta = 9°$, the symmetry of the flow is removed and the intensity of the turbulent formation is significantly changed. The size of the two eddies in the propeller disc area is modified

becoming more notable in diagonal direction of the incoming flow and diminishes until almost disappearing on the incident board. At the same time, the oblique vortex originating from the bow area and evolving in the drift direction adds to the boundary structure manifested in the way of it, amplifying its presence.

Figure 8, also, illustrates the hydrodynamic impact of the active propeller on the axial velocity distribution at $x = 0.9825$ L_{pp}. In both scenarios of $\beta = 0°$ and $\beta = 9°$, the imprint of the propulsion unit is found to be highly noticeable in the disc area. Consequently, the two vortices that create the "hook"-like shape are partially removed and the non-dimensional axial velocity, u, escalates reaching the speed of the ship at certain points. Thus, the rotational and accelerating effect of the propeller is revealed. However, it should be noted that at $\beta = 0°$, in the hub area, there is a low-intensity vortical formation that can, confidently, be attributed to the two horseshoe eddies observable in the bare hull analysis. The right-hand propeller directs this circular flow to portside. Moreover, at $\beta = 9°$, a remnant of the "hook" is, also, identified in the starboard side of the contour lines, whereas, the bow formed vortex remains unchanged. Outside the area of the disc, there are no significant changes in either the distribution or the values of u. The only exception is the manner in which the contour lines converge towards the upper part of the propulsion unit.

C. Flow Downstream of the Propeller Plane

Figures 9 and 10 depict the evolution of the flow downstream of the propeller plane. The analyzed sections are in correspondence with the axis of the rudder at $x = 1.00$ L_{pp} and behind the rudder at $x = 1.10$ L_{pp}. The results are presented for the bare hull configuration when the ship is on a straight course or engaged in a static maneuvering motion, as well as for the hull equipped with an operating propeller under the same inflow conditions ($\beta = 0°$ and $\beta = 9°$).

In the case of the bare hull, the figures corresponding to the zero drift condition, confirm the presence of the boundary and "hook"-like pairs of vortices. Even if, inside the disc area, the values of the axial velocity are higher than the ones in the upstream sections, the turbulence of the flow is still significant. As rendered by the contour lines, at $x = 1.10$ L_{pp}, the horseshoe shape disappears and the two joined eddies split manifesting a symmetrical evolution until vanishing [23]. In the same plane, it is observed that the side vortices narrow in the upper part of the propulsion unit. In terms of magnitude, the values of the axial velocity are greater than the upstream ones and increase proportionally with the distance from the ship hull.

At 9° drift, the flow no longer maintains its symmetry with respect to the CL. The intensity of the two pairs of bilge vortices increases on the side opposite to the incident board and decreased until disappearing in the incident side of the body. The bow vortex developed along the drift angle direction contributes to this diagonal development of the flow. Its addition to the already existing patterns augments the axial velocity with at least an order of magnitude.

As Figure 10 shows, the propeller imprints an acceleration and rotational effect on the flow. Slightly noticeable upstream of the propulsion unit, these influences are more strongly felt in the propeller plane and downstream, at $x = 1.00$ L_{pp} and $x = 1.10$ L_{pp}. It is worth mentioning that all these happen in the disc area, being almost non-existent outside it. Thus, for the zero drift condition, the non-dimensional axial velocity u reaches the maximum value of 1.2 U at $x = 1.00$ L_{pp}, compared to the maximum speed of 0.8 U recorded for the bare hull configuration. Although with an order of magnitude smaller, the utmost value of 1.1 U at $x = 1.10$ L_{pp} exhibits the same outcome.

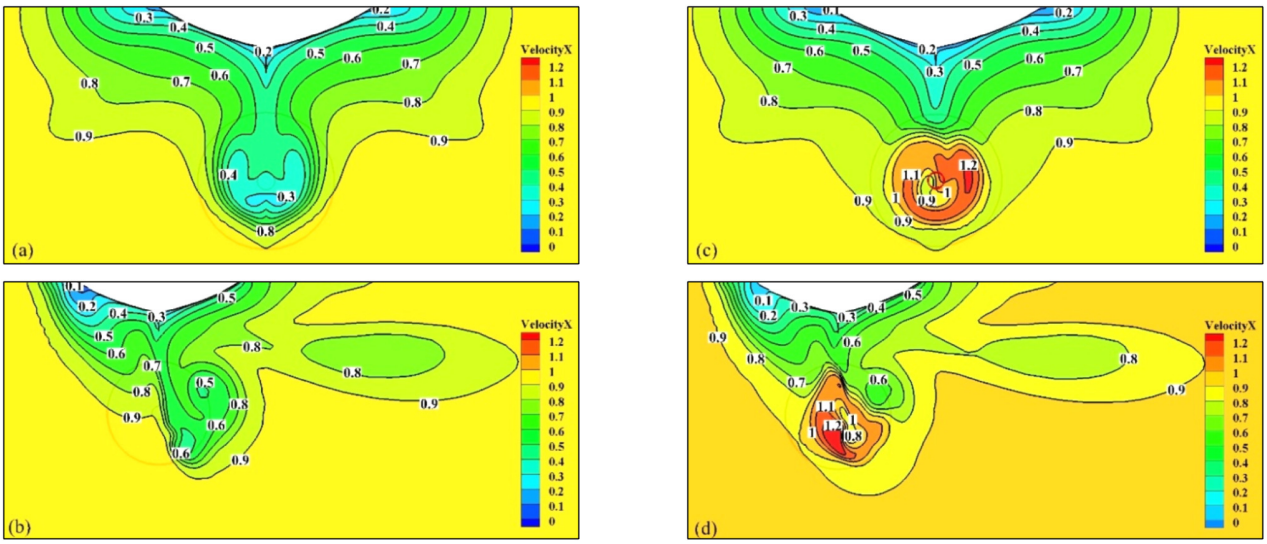

Fig. 9. Axial velocity distribution downstream of the propeller plane at $x = 1.00$ L_{pp} for: (a) bare hull and $\beta = 0°$, (b) bare hull and $\beta = 9°$, (c) hull with propeller and $\beta = 0°$, and (d) hull with propeller and $\beta = 9°$.

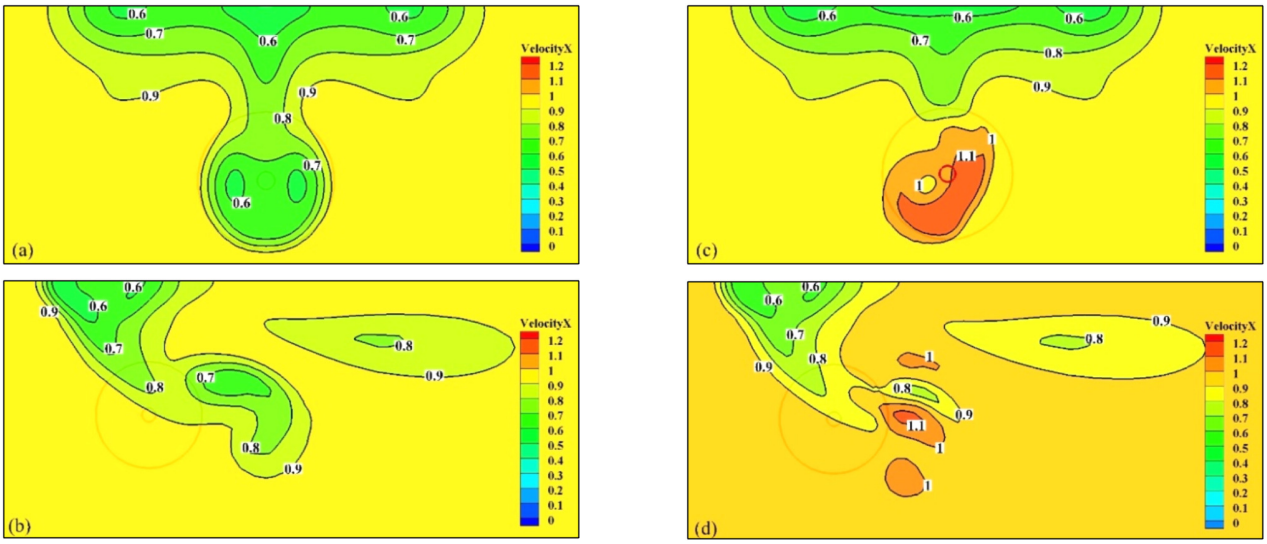

Fig. 10. Axial velocity distribution downstream of the propeller plane at $x = 1.10\ L_{pp}$ for: (a) bare hull and $\beta = 0°$, (b) bare hull and $\beta = 9°$, (c) hull with propeller and $\beta = 0°$, and (d) hull with propeller and $\beta = 9°$.

By rotating and accelerating the flow, the propeller removes or modifies the vortical formations identified for the bare hull case. Thus, in the active disc area, the "hook"-like eddies are removed, whereas, outside this zone, the contour lines tighten at the top of the propulsion unit modifying the flow pattern. The values of the axial velocities are unchanged.

For 9° drift, Figure 9(d) highlights that even in the presence of the disc, the vortical character of the flow is preserved. At $x = 1.00\ L_{pp}$, the distribution of the contour lines show in the starboard upper part of the propeller a small vortex that is what is left of the "hook"-like shape, whereas the starboard side and the bow formed eddies join without suffering any change in their values. Further, at $x = 1.10\ L_{pp}$, the flow is still under the influence of the incident flow, and the bow vortex, although separate from the side one that has vanished, still keeps its order of magnitude. Withal, the rest of the "hook" is still obvious together with the rotational and propulsive effect of the unit.

IV. CONCLUSIONS

Given the high expectations for GHG reduction from ships and their connection with the propulsion system, the current study highlights the need for a better understanding of the hydrodynamics of the propeller's operating field, when the ship is on a straight course or during a maneuvering motion. Furthermore, it is emphasized that in order to make informed design choices, for new projects or retrofits, which can contribute to pollution reduction, it is absolutely necessary to understand the interactions that occur between the stern flow turbulent phenomena and the active propeller.

For a clearer picture of the analyzed situations, the study exclusively focuses on the axial velocity distribution in the aft part of the ship, with both the bare hull and the hull with propeller configurations being considered. In the case of each constructive ensemble, five transversal sections distributed along the ship hull at various positions relative to the propeller plane were examined and specific and common conclusions were drawn. A qualitative validation of the numerical technique used for obtaining the axial velocity distribution demonstrates the accuracy of the results.

Thus, it can be concluded that the distinctive design of these type of full-bodied tankers characterized by large block coefficient and pronounced bow and stern curvature, generate ample vortical motions that develop along the ship hull influencing the propeller inflow. Symmetrical in relation to the CL, when engaged on a straight-ahead route, the turbulent flow intensifies, in the board opposite to the board of incidence, for non-zero drift angles. In essence, two pairs of eddies appear in the bilge area at zero incidence, whereas a third vortex, started from the bow area, adds to the flow during drift. All these rotational motions imprint the stern flow hydrodynamics, manifesting from upstream of propeller until far downstream.

When introduced in the study, the propeller effect is weakly felt in the upstream planes where the flow pattern is almost unchanged in comparison with the bare hull situation. Its accelerating effect that determines an undesired increase of ship resistance is, though, present. Much more observed in the propeller plane and downstream, it causes a majoring of the axial velocities in the unit operating area as well as a reduction or even removal of the "hook"-like vortices. In addition, the tightening of the contour lines is visible at the top of the propulsion unit.

Nonetheless, the analysis highlights the fact that, outside the disc area, the values of the axial velocities are unchanged, with their distribution demonstrating a minor asymmetry. It is clear that the vortical character of the flow due to the intricacy of its surfaces and to the drift motion is way more influential.

In summary, the depicted results underscore the importance of accurately considering the turbulent stern flow hydrodynamics in both the new ship design and its optimization. Their knowledge allows the best solutions for

reducing greenhouse gas emissions while improving the propulsion and maneuvering performances of the ship. Thus, beside the valuable insights provided for the pollution-propulsion efficiency dependence, the obtained results could also support the "development and implementation of standards for a ship's maneuverability, particularly for large ships and ships carrying dangerous goods in bulk" [26].

In essence, the present research, offers an alternative that can be implemented as early as during the preliminary design phases for both testing and optimization purposes. The CFD based techniques can mitigate the time and financial costs of experimental modelling.

As a general conclusion, the study provides a novel and significant contribution to the naval architecture field by providing a comprehensive analysis of the intricate phenomena describing the stern flow hydrodynamics, for the ship with or without propeller, under various incident flow conditions. The novelty of the research lies in the systematic approach of the "static drift" virtual PMM tests, with the complete set of numerical solutions reported for this problem being able to assist the propulsion unit design and optimization process by offering a cost-effective and accurate alternative to experimental modelling.

ACKNOWLEDGMENT

The authors would like to express their gratitude to Prof. Dr. Adrian Lungu for his guidance, support, and insightful suggestions.

REFERENCES

[1] "2023 IMO Strategy on Reduction of GHG Emissions from Ships," *IMO*. https://www.imo.org/en/OurWork/Environment/Pages/2023-IMO-Strategy-on-Reduction-of-GHG-Emissions-from-Ships.aspx.

[2] *Guidelines for Determining Minimum Propulsion Power to Maintain the Manoeuvrability of Ships in Adverse Conditions. MEPC.1/Circ.850/ Rev.3.* London, UK: IMO, 2021.

[3] *Review of Maritime Transport 2023. United Nations Conference on Trade and Development, 2023.*

[4] *Fourth IMO GHG Study 2020. Full Report.* London, UK: IMO, 2021.

[5] E. V. Palconit and M. L. S. Abundo, "Transitioning to Green Maritime Transportation in Philippines," *Engineering, Technology & Applied Science Research*, vol. 9, no. 1, pp. 3770–3773, Feb. 2019, https://doi.org/10.48084/etasr.2457.

[6] M. Amoraritei and G. Constantin, "A study on ship propulsion performances considering EEDI regulations," *Annals of "Dunarea de Jos" University of Galati. Fascicle XI Shipbuilding*, vol. 40, pp. 43–48, Dec. 2017.

[7] Y. Zhang, B. Winden, H. R. D. Ojeda, D. Hudson, and S. Turnock, "Influence of drift angle on the propulsive efficiency of a fully appended container ship (KCS) using Computational Fluid Dynamics," *Ocean Engineering*, vol. 292, Jan. 2024, Art. no. 116537, https://doi.org/10.1016/j.oceaneng.2023.116537.

[8] SIMMAN 2008, "Workshop on Verification and Validation of Ship Manoeuvring Simulation Methods." http://www.simman2008.dk/ contents.htm.

[9] L. Larsson, F. Stern, and M. Visonneau, *Numerical Ship Hydrodynamics: An assessment of the Gothenburg 2010 Workshop.* New York, NY, USA: Springer, 2013.

[10] SIMMAN 2014, "Workshop on Verification and Validation of Ship Manoeuvring Simulation Methods." https://simman2014.dk/.

[11] Tokyo 2015, "Tokyo 2015 A Workshop on CFD in Ship Hydrodynamics." https://www.t2015.nmri.go.jp/.

[12] SIMMAN 2020, "Workshop on Verification and Validation of Ship Manoeuvring Simulation Methods." https://simman2020.kr/index.php.

[13] E. Alizadeh, A. Maleki, and A. Mohamadi, "An Investigation of the Effect of Ventilation Inlet and Outlet Arrangement on Heat Concentration in a Ship Engine Room," *Engineering, Technology & Applied Science Research*, vol. 7, no. 5, pp. 1996–2004, Oct. 2017, https://doi.org/10.48084/etasr.1288.

[14] A. C. Mangra, "Design and Numerical Analysis of a Micro Gas Turbine Combustion Chamber," *Engineering, Technology & Applied Science Research*, vol. 10, no. 6, pp. 6422–6426, Dec. 2020, https://doi.org/10.48084/etasr.3835.

[15] C. D. Simonsen and F. Stern, "Flow pattern around an appended tanker hull form in simple maneuvering conditions," *Computers & Fluids*, vol. 34, no. 2, pp. 169–198, Feb. 2005, https://doi.org/10.1016/j.compfluid. 2004.05.001.

[16] C. D. Simonsen and F. Stern, "RANS Maneuvering Simulation of Esso Osaka With Rudder and a Body-Force Propeller," *Journal of Ship Research*, vol. 49, no. 2, pp. 98–120, Jun. 2005, https://doi.org/ 10.5957/jsr.2005.49.2.98.

[17] C. D. Simonsen and F. Stern, "Flow structure around manoeuvring tanker in deep and shallow water," in *26th ONR Symposium on Naval Hydrodynamics*, Rome, Italy, 2006.

[18] S. R. Turnock, A. B. Phillips, and M. Furlong, "Urans simulations of static drift and dynamic manoeuvres of the KVLCC2 tanker," in *Workshop on Verification and Validation of Ship Manoeuvring Simulation Methods*, Lyngby, Denmark, Apr. 2008.

[19] A. Lungu and F. Pacuraru, "Numerical Study of the Hull-Propeller-Rudder Interaction," *AIP Conference Proceedings*, vol. 1168, no. 1, pp. 693–696, Sep. 2009, https://doi.org/10.1063/1.3241559.

[20] O. Marcu and A. Lungu, "Numerical investigation of the flow around the KVLCC2 hull in static drift motion," *AIP Conference Proceedings*, vol. 1479, no. 1, pp. 185–188, Sep. 2012, https://doi.org/10.1063/1.4756093.

[21] Y. Zhang, D. Hudson, B. Winden, and S. Turnock, "Evaluating the effects of drift angle on the self-propelled ship using Blade Element Momentum Theory," in *23rd Numerical Towing Tank Symposium*, Mulheim an der Ruhr, Germany, Oct. 2021, pp. 159–164, https://doi.org/10/21.

[22] Y. Zhang, B. Winden, D. Hudson, and S. Turnock, "Hydrodynamic performance of a self-propelled KCS at angle of drift including rudder forces," in *24th Numerical Towing Tank Symposium*, Zagreb, Croatia, Oct. 2022.

[23] O. Marcu, "Contributions to the study of the flow around the hull-propeller-rudder configuration," Ph.D. dissertation, University of Galati, Galati, Romania, 2012.

[24] T. B. Gatski and C. G. Speziale, "On explicit algebraic stress models for complex turbulent flows," *Journal of Fluid Mechanics*, vol. 254, pp. 59–78, Sep. 1993, https://doi.org/10.1017/S0022112093002034.

[25] W. J. Kim, S. H. Van, and D. H. Kim, "Measurement of flows around modern commercial ship models," *Experiments in Fluids*, vol. 31, no. 5, pp. 567–578, Nov. 2001, https://doi.org/10.1007/s003480100332.

[26] *Resolution MSC.137(76) (adopted on 4 December 2002). Standards for Ship Manoeuvrability. London, UK: IMO, 2002.*